

## Article

# Combustion Behavior and Microstructure of TC17 Titanium Alloy under Oxygen-Enriched Atmosphere

Cheng Zhang<sup>1,\*</sup>, Peng Xing<sup>2</sup>, Zhibin Li<sup>1</sup>, Congzhen Wang<sup>1</sup>, Caihong Dou<sup>1</sup>, Yuxuan Jiao<sup>1</sup>, Jianjun Li<sup>1</sup>, Biao Wang<sup>2</sup>, Guangyu He<sup>3</sup> and Jinfeng Huang<sup>1</sup>

<sup>1</sup> State Key Laboratory for Advanced Metals and Materials, University of Science and Technology Beijing, Beijing 100083, China

<sup>2</sup> AECC Sichuan Gas Turbine Establishment, Chengdu 610500, China

<sup>3</sup> School of Mechanical Engineering, Xi'an Jiaotong University, Xi'an 710049, China

\* Correspondence: zhangcheng@ustb.edu.cn

**Abstract:** TC17 titanium alloy is widely used in the aerospace industry, but its combustion behavior and microstructure after combustion are rarely investigated. Herein, the ignition critical oxygen pressure, combustion velocity, and microstructure after the combustion of TC17 titanium alloy were investigated by promoted ignition combustion tests under an oxygen-enriched environment. The results indicated that there were three stages, ignition, splash, and flame propagation, for the combustion process of the TC17 alloy. As compared to TC11 titanium alloy, the TC17 titanium alloy exhibited a similar ignition critical oxygen pressure with the same size, but an obviously faster burning rate, which followed a power law relationship with the oxygen pressure. The segregation of Cr, Mo, and Al was observed in the interdendritic phase of the melting zone and the interface between the melting zone and the heat-affected zone. The segregation of Cr at the liquid/solid interface can be responsible for accelerating the burning kinetic of the TC17 alloy by decreasing the interfacial temperature.

**Keywords:** TC17 alloy; combustion behavior; combustion microstructure; combustion velocity



**Citation:** Zhang, C.; Xing, P.; Li, Z.; Wang, C.; Dou, C.; Jiao, Y.; Li, J.; Wang, B.; He, G.; Huang, J. Combustion Behavior and Microstructure of TC17 Titanium Alloy under Oxygen-Enriched Atmosphere. *Metals* **2023**, *13*, 1020. <https://doi.org/10.3390/met13061020>

Academic Editor: Tullio Monetta

Received: 8 March 2023

Revised: 9 April 2023

Accepted: 15 May 2023

Published: 26 May 2023



**Copyright:** © 2023 by the authors. Licensee MDPI, Basel, Switzerland. This article is an open access article distributed under the terms and conditions of the Creative Commons Attribution (CC BY) license (<https://creativecommons.org/licenses/by/4.0/>).

## 1. Introduction

Titanium alloys are regarded as promising structural materials in the aero industry due to their superior properties, such as low density, high specific strength, and high corrosion resistance, etc., [1]. However, they also suffer from risk of combustion in harsh conditions, such as oxygen-rich atmosphere or friction at elevated temperatures [2,3]. Due to the high combustion heat and low thermal conductivity of titanium, once these alloys are ignited, the combustion reaction can scarcely be extinguished and it spreads to the whole component in less than 30 s, which is known as “titanium fire” [4]. A number of accidents have resulted from the “titanium fire” ever since titanium alloys have been employed extensively in aeroengines.

The combustion behavior and mechanisms of titanium alloys have been examined in numerous studies. Littmen et al. [5] studied the combustion behavior of pure titanium; they found that the critical oxygen pressures for ignition decreased with the temperature increasing. Since titanium alloys have extremely high combustion temperatures, it has been reported that their combustion process involves a liquid-phase combustion reaction [6–8], meaning that the alloys are melted into liquid phase during combustion. The peak temperature of flame for titanium alloys has been reported to be 3000–3400 K, following an explosion and bright light phenomenon [9,10]. The combustion mechanism of titanium alloys has also been reported to be related to the transformation of surface oxides. According to Schutz [11], the surface oxides were fractured or even melted due to the reaction heat accelerating the oxidation reaction and raising temperatures in the reaction zones. Bolobov [12,13] also suggested that the combustion was related to the fracture of surface

oxides, owing to the volume contract during the transformation of different oxides. As surface oxides are fractured and peeled off, the oxidation process will become more active. The morphology and structures of the surface oxides also have an impact on combustion behaviors. Some have also suggested that a succession of oxidation processes between a high valent oxide, such as  $\text{TiO}_2$ , and sub-oxides, such as  $\text{TiO}$  and  $\text{Ti}_2\text{O}_3$ , may result in the combustion [10,14].

Many studies on the impact of alloyed elements on the combustion behavior have been conducted to increase the burn-resistance of titanium alloys. Promoted ignition combustion (PIC) methods with varying oxygen pressure and contents have been used to quantitatively study the combustion behavior of the TC4 (Ti-6Al-4V), TC11 (Ti-6.5Al-3.5Mo-1.5Zr-0.3Si), and  $\text{Ti}_2\text{AlNb}$  alloys [14–16]. The combustion velocity of TC4 is higher than that of TC11, which is attributed to the enriched distribution alloying elements close to the interface of the melting zone and matrix, i.e., V for the TC4 alloy and Mo, Zr, and Si for the TC11 alloy [14]. It has also been reported that the Al and V alloying elements in TC4 alloy cannot prevent the oxygen diffusion into the alloy matrix during the combustion process [17]. The combustion behavior and mechanism of the  $\text{Ti}_2\text{AlNb}$  alloy are compared with the TC11 alloy. Although the ignition temperatures of the two alloys show little difference, the combustion velocity of  $\text{Ti}_2\text{AlNb}$  is faster than that of TC11 alloy. It has been proposed that this difference is related to the different locations of the enrichments of the Nb and Mo elements, and the decomposition of the O phase in the heat-affected zone [15]. In addition to the typical  $\alpha + \beta$  dual-phase titanium alloys, the combustions of the Ti-Cr-V and Ti-Cu alloys are also studied. The ignition temperatures of Ti40 (Ti25V-15Cr) are higher than those of TC4 due to the decomposition and volatilization of  $\text{V}_2\text{O}_5$ , but the combustion velocity of Ti-25V-15Cr is faster than that of TC4, attributed to the different migration way of the solid–liquid interface [18]. Studies have also reported that the burn resistance of titanium alloys is improved by the addition of Cu due to the reduction in heat generation and the improvement of heat transmission. For instance, it has been reported that the Ti14 (Ti-1Al-13Cu-0.2Si) alloy exhibits a better burn resistant capability with lower combustion velocity and flame height, and it is related to the suppressed diffusion of oxygen due to the formation of a multiple-layer structure with a Cu-enrichment in the burn heat-affected zone [19,20]. Compared with the typical  $\alpha + \beta$  dual-phase titanium alloys such as TC4 and TC11, TC17 (Ti-5Al-2Sn-2Zr-4Mo-4Cr) is a kind of near  $\beta$  type  $\alpha + \beta$  dual-phase titanium alloy by the addition of  $\beta$ -phase strengthening elements, such as Cr and Mo, it has been widely used in high-pressure compressor blades and other parts of aero-engines, which require high bearing capacity [21,22]. However, the combustion behavior of the TC17 alloy is rarely investigated at present, particularly the ignition conditions and combustion kinetics compared to the other titanium alloys, which is critical for the safe use of the TC17 alloy in the application of aero industries.

In this work, the combustion behavior of the TC17 alloy (Ti-5Al-2Sn-2Zr-4Mo-4Cr), including ignition temperature, threshold oxygen pressure, and combustion kinetics, is investigated by the promoted ignition–combustion (PIC) tests. The microstructure after extinguishing combustion is further analyzed, and the impact of alloying elements on the combustion behavior is further discussed.

## 2. Experimental Materials and Methods

### 2.1. Experimental Material

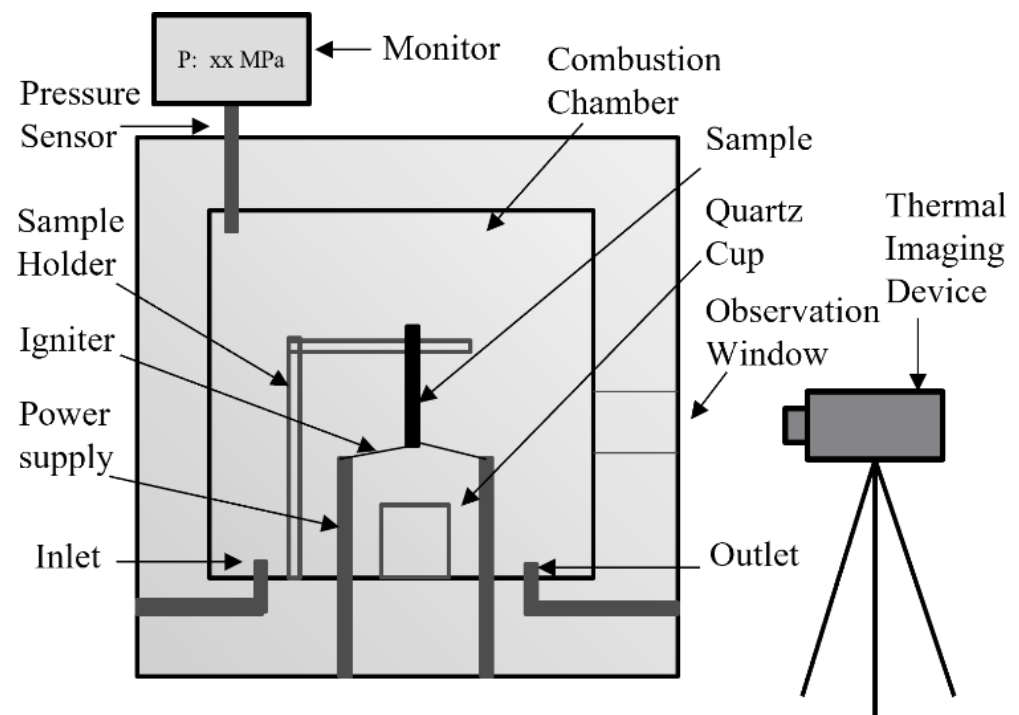
The TC17 titanium alloy (Ti-5Al-2Sn-2Zr-4Mo-4Cr, wt.%) bar was prepared by vacuum melting, hot rolling, and annealing treatment. The chemical composition of the TC17 alloy bar is listed in Table 1. Then, the alloy bar was machined into rod samples with dimensions of  $\Phi 3.2 \times 70$  mm through wire cutting and surface polishing.

**Table 1.** Chemical composition of TC17 alloy.

wt.%	Al	Mo	Zr	Sn	Cr	Fe	Ti
	4.6	4.1	1.9	2.0	4.0	0.15	Bal.

### 2.2. Promoted Ignition–Combustion (PIC) Test

The PIC tests that were carried out were widely used in oxygen-enriched atmosphere, and the test procedures are described in detail in reference [3]. The variations of temperature during the combustion process were recorded by using thermal imaging (MCS640, LUMASENSE TECHNOLOGIES, Santa Clara, CA, USA). The experimental atmosphere was oxygen with high purity (99%). The chamber of the equipment was pumped to a vacuum of  $10^{-1}$  to  $10^{-2}$  Pa, and then the gaseous oxygen was pumped into the equipment at the oxygen pressure from 0.1 MPa to 0.5 MPa. The quartz tubes with an internal diameter of 3.2 mm and a length of 20 mm were put on the samples at positions corresponding to the sample lengths of 10, 20, 30, and 40 mm for the determination of burning velocity in different stages. The combustion process slowed down and was terminated at the set position due to the oxygen being isolated by the ceramic ring and argon gas. The combustion velocity was obtained at different lengths by recording the remaining length and time. The equipment of the PIC test and the combustion process are shown in Figure 1. Each test was repeated three times to ensure the reliability of the experimental data.

**Figure 1.** The diagram of promoted ignition–combustion (PIC) device.

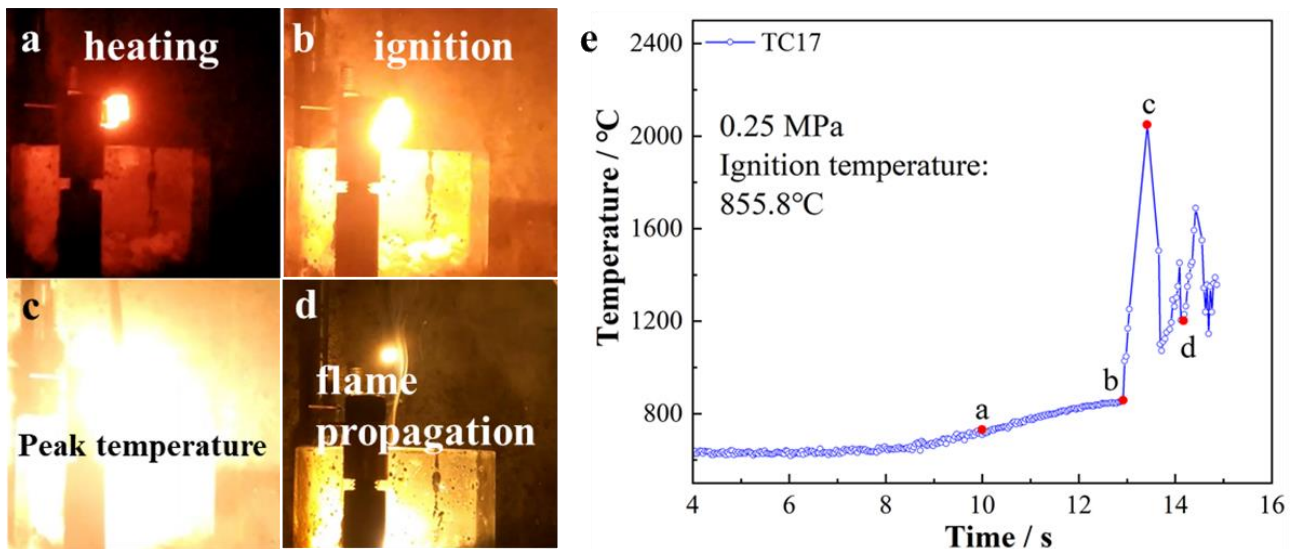
### 2.3. Microstructural Characterization

The burned specimens were cut along long longitudinal sections, polished, and etched with a mixed solution of 10 vol.% HF, 30 vol.% HNO<sub>3</sub>, and 10 vol.% H<sub>2</sub>O. The phase structure of combustion products was determined by X-ray diffraction (Rigaku TTR3, Tokyo, Japan), using Cu K $\alpha$  radiation with a step of 0.02° and counting time of 1 s/step. The microstructure and chemical composition of different combustion reaction zones was observed by the field emission scanning electron microscope (SEM) with an operating voltage of 20 keV (Supra 55, Zeiss, Oberkochen, Germany), equipped with energy-dispersive spec-

trometry (EDS). The chemical composition distribution of different combustion reaction zones was analyzed using an electron probe micro-analyzer (EPMA-1720H, Kyoto, Japan).

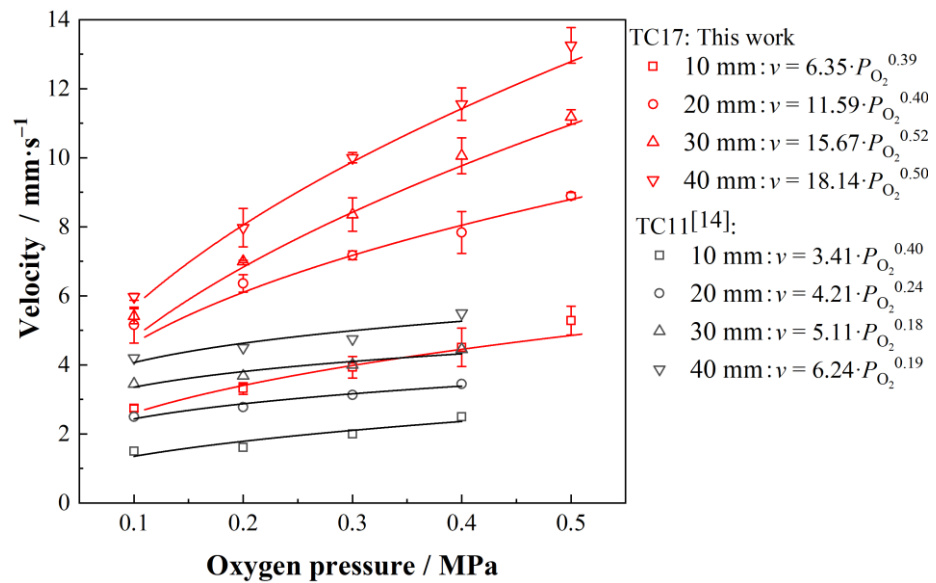
### 3. Results

Figure 2 shows the in situ observation of the combustion process of TC17 titanium alloy (Ti-5Al-2Sn-2Zr-4Mo-4Cr) and the corresponding temperature curve. It can be observed in Figure 2a that there are three steps to the TC17 alloy's combustion process, i.e., the ignition, splash (or explosion), and flame propagation processes. It is similar to those of TC4 (Ti-6Al-4V) and TC11 (Ti-6.5Al-3.5Mo-1.5Zr-0.3Si) alloys, which were described in detail in our previous study [14]. The corresponding temperature curve in Figure 2b shows that the surface temperature increases rapidly from the ignition temperature (855.8 °C) to the peak temperature (2047.5 °C) within only 0.5 s when the alloy is ignited. After the splash stage, the steady propagation of the flame is observed, with the formation of a molting droplet. Additionally, the threshold oxygen pressure of the TC17 alloy is determined as 0.09 MPa, which is close to that of 0.07 MPa for the TC11 alloy.



**Figure 2.** (a–d) the in situ observation on combustion of TC17 alloy and (e) the corresponding temperature curve under 0.25 MPa.

The combustion velocity of the TC17 alloy is obtained from the combustion length and time, and the curves of combustion velocity with oxygen pressure are plotted, as shown in Figure 3. As a comparison, the combustion velocity of the TC11 alloy is also plotted; the data were obtained from previous work [14]. It can be seen in Figure 3 that the combustion velocity of the TC17 samples increases when oxygen pressure rises from 0.1 MPa to 0.5 MPa. Similar to that of TC11, the combustion velocity rises with the sample length, suggesting that combustion is a self-accelerating phenomenon. It should be noted that the combustion velocity of TC17 with the same length is significantly higher than that of TC11, and the self-accelerating phenomenon is more sensitive in TC17. Additionally, it can be seen that the combustion velocity  $v$  and with oxygen pressure  $P_{O_2}$  follows a power law relationship for both the TC17 and TC11, where the rate constant and exponent of TC17 are larger than that of TC11.



**Figure 3.** The combustion velocity vs. oxygen pressure relationship of TC17 alloy [14].

Combustion products of TC17 include droplet, volatile, and molten pool. The XRD analysis of combustion products are carried out, as shown in Figure 4. It has been found that the droplet is mainly composed of  $\text{Ti}_2\text{O}_3$ ,  $\text{TiO}$ ,  $\text{TiO}_2$ ,  $\text{Ti}_3\text{O}_5$ ,  $\text{Al}_2\text{O}_3$ ,  $\text{Sn}$ , and  $\text{Cr}_2\text{O}_3$ . The molten pool contains  $\text{Ti}_2\text{O}_3$ ,  $\text{TiO}$ ,  $\text{TiO}_2$ ,  $\text{Ti}_2\text{O}$ , and  $\text{ZrO}_{0.35}$ . The volatile consists of  $\text{Ti}_3\text{O}_5$ ,  $\text{TiO}_2$ ,  $\text{SnO}_2$ , and  $\text{MoO}_3$ , which indicates that the combustion temperature is higher than these oxides.

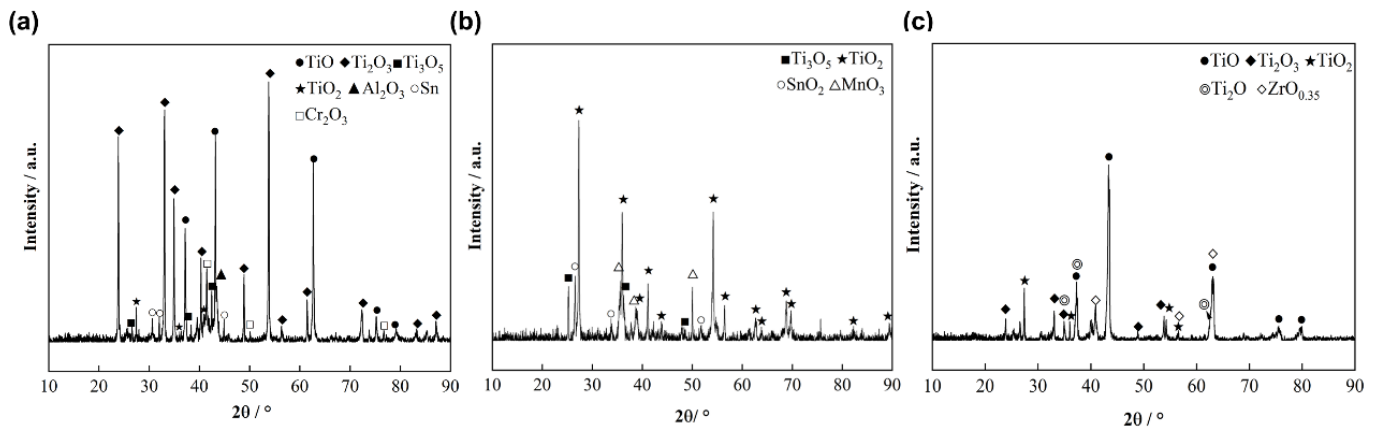


**Figure 4.** XRD results of combustion products TC17 alloy: (a) droplet, (b) volatile, and (c) molten pool.

Figure 5 depicts the microstructure of the TC17 alloy after extinguishing the combustion process. After combustion, the microstructure of the TC17 alloy contains three regions, including the oxide zone, melting zone, and heat-affected zone. Many cracks and cavities can be seen in the oxide zone, as shown in Figure 5a. The formation of cracks can be related to the internal stress caused by the shrinkage during the solidification process. The oxide zone contains two different phases, i.e., the dark gray oxide matrix phase (Phase 1) and the white network phase (Phase 2). The chemical compositions of Phase 1 and Phase 2 are obtained by EDS, as listed in Table 2. Figure 5e further shows the distribution of elements in oxide zone. It can be observed that the dark gray oxide matrix phase (Phase 1) is mainly the mixture of titanium oxides. The white network phase (Phase 2), which differs from Phase 1, which is enriched in Zr, Sn, Mo, and Cr, suggests that Ti was oxidized before these elements, which is compatible with the XRD results of the molten pool seen in Figure 4.

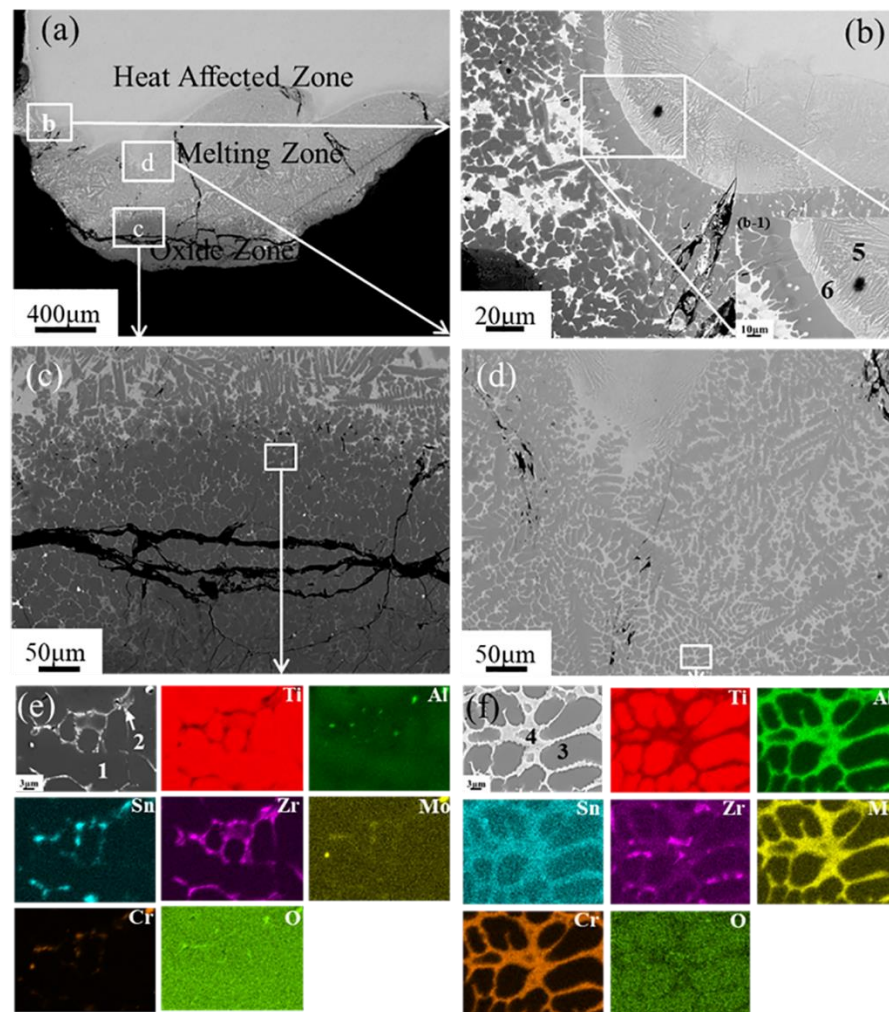


**Figure 5.** Microstructure of TC17 alloy. (a) Overall morphology, (b) heat-affected zone, (c) oxide zone, (d) melting zone, (e) the EDS mapping of the marked area in (c), (f) the EDS mapping of marked area in (d). (b-1) is the local magnification in (b). The number from 1–6 represents the positions of EDS analysis.

**Table 2.** Chemical concentration of different phases for TC17 alloy.

Region	Composition						
	Ti	Al	Sn	Zr	Mo	Cr	O
Phase 1 (at %)	39.93	2.87	0.02	0.09	0	0.07	57.02
Phase 2 (at %)	33.4	1.46	3.27	14.92	0.41	1.32	45.23
Phase 3 (at %)	63.07	3.96	0.45	0	0	0.56	31.96
Phase 4 (at %)	50.54	18.92	1.14	0.7	3.29	9.88	15.53
Phase 5 (at %)	64.43	8.09	0.8	1.1	1.58	3.6	20.4
Phase 6 (at %)	51.02	15.2	0.98	1.08	4.47	7.77	19.48

Figure 5b depicts the morphology of the melting zone. Figure 5d is the enlarged view of Figure 5b. A typical dendritic solidification structure can be observed in the melting zone. The element mapping of the dendritic phase (Phase 3) and interdendritic phase (Phase 4) are shown in Figure 5f. As shown in Table 2, a high concentration of oxygen of approximately 31 at.% is determined by EDS in Phase 3, where the atomic ratio of Ti and O in Phase 3 is close to 2:1. According to the Ti-O phase diagram, such an increasing solid solubility of dendritic suggests that a peritectic transformation between liquid titanium and  $\alpha$  solid solution into TiO oxide is involved. As illustrated in Figure 5f, the enrichment

of Al, Mo, and Cr is seen in the interdendritic phase (Phase 4). The oxygen content in the interdendritic phase, which is substantially lower than that of the dendritic phase, and can be attributed to the segregation of elements that shorten the region of the phase, is around 15%, as listed in Table 2. It can be also noted that the relative ratio between interdendrite and dendrite decreases far away from the liquid/solid interface, suggesting the diffusion of Al, Mo, and Cr toward the liquid/solid interface in the melting zone.

Because of the high temperature brought on by the heat conduction of the melting zone, as shown in Figure 5b, coarse grains can be observed in the heat-affected zone. The boundary between the heat-affected zone and the melting zone is clearly visible, similar to the TC11 and TC4 alloys, as shown in the enlarged image in Figure 5b, and it may be related to the peritectic reaction between the liquid and solid phases. An enrichment of alloying elements is found from the matrix to the interface between the heat-affected zone and melting zone. The EDS analysis in Table 2 shows that Point 6 in the heat-affected zone contains 15.2 at % Al, 4.47 at % Mo, and 7.77 at % Cr near the interface, which is about twice that near the matrix (Point 5). The segregation of Al, Mo, and Cr at the interface is also shown by the EPMA element mapping in Figure 6, which will be discussed in detail in the discussion section.

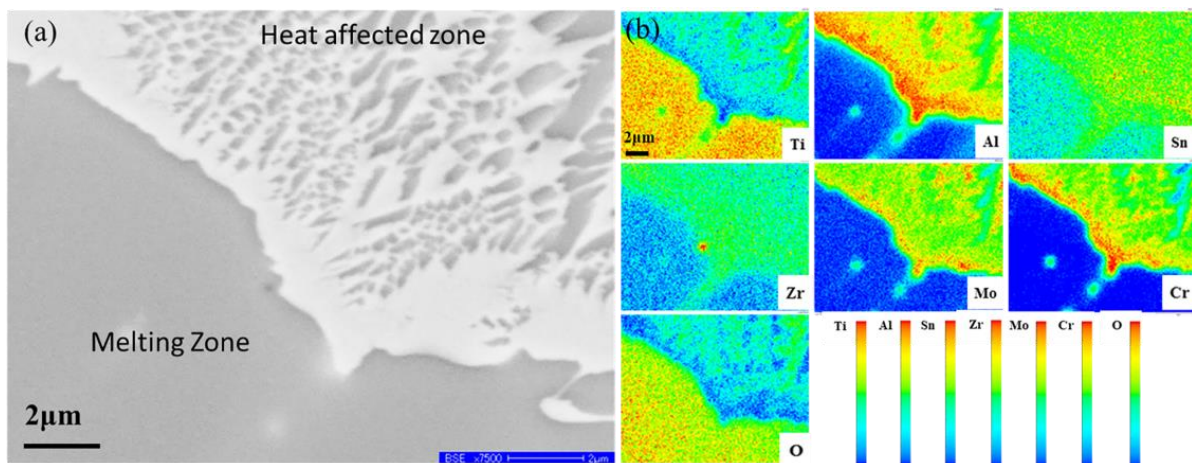


**Figure 6.** Microstructure of the front of the heat-affected zone for TC17 alloy: (a) SEM micrograph, (b) EPMA mapping.

#### 4. Discussion

Compared to the TC11 alloy, the TC17 alloy is a near  $\beta$  type  $\alpha + \beta$  dual-phase titanium alloy due to more addition of  $\beta$ -phase stable elements, such as Cr and Mo. It has an impact on both the combustion behavior and microstructure evolution of the TC17 alloy during combustion.

According to in situ combustion observations (Figure 2), the combustion of TC17 involves three steps, including ignition, splashing, and flame propagation, which is similar to the combustion of TC4 and TC11 alloys [14]. The PIC experiments also show that even though the TC17 alloy's threshold ignition pressure is similar to that of the TC11 alloy, it burns with a substantially higher velocity under conditions of equal oxygen pressure and combustion length (see Figure 3). A very high oxygen content of around 31 at. % is confirmed in the dendritic phase of the melting zone for the microstructure of the TC17 alloy after combustion, as shown in Table 2. Such a growing solid solubility of dendrite implies that a peritectic transformation, i.e., liquid phase +  $\alpha$  phase  $\rightarrow$  TiO, can be engaged in the combustion of the TC17 alloy, which is similar to other typical titanium alloys that contain the  $\alpha$  phase, such as TC4 and TC11 in our previous work [14–16]. Additionally, the self-accelerating combustion behavior of the TC17 has been observed, as shown in Figure 3. Such a phenomenon has also been observed in TC4, TC11, and Ti14 alloy in references [14,15,20], which can be attributed to the extremely high combustion

heat of titanium alloys, offering sufficient energy as the driving force for the acceleration of the reactions.

The addition of  $\beta$ -phase stable elements, such as Cr, can be the reason for the rapid combustion kinetics of the TC17 alloy. Because of the periodic formation of combustion areas and droplets, as observed in the PIC tests, it is reasonable to consider the flame propagation of the TC17 and TC11 alloys as a steady process. By equating the heat flux on the liquid side to that on the solid side, the migration rate  $v$  of the interface between solid and liquid can be expressed as [23]  $v = \frac{Ah(T_b - T_m)}{\rho\{c(T_m - T_s) + q\}}$ , which is based on the energy conservation law, where  $A$  is the parameter corresponding to the configuration of the interface,  $h$  is the heat transfer rate at the interface,  $T_b$  is the molten mass temperature,  $T_m$  is the temperature at the interface that is equal to the metal melting temperature,  $\rho$  is the density of titanium alloy,  $c$  is the specific heat capacity,  $T_s$  is the temperature of solid alloy, and  $q$  is the latent heat of melting process. The combustion velocity of different titanium alloys can be compared and explained by the equation of the analysis of alloying characteristics on kinetic parameters.

According to this equation, the interfacial temperature  $T_m$  is the primary cause of the difference of migration rate  $v$  between TC17 and TC11. Table 3 compares the major physical characteristics of TC17 and TC11 alloys, including  $q$ ,  $h$ ,  $c$ , and  $\rho$ , based on references [24–26]. It can be seen that the TC17 and TC11 alloys have similar values for all of these characteristics. However, as illustrated in Figure 6, during the combustion process, the segregation of the  $\beta$ -phase stable element Cr is seen at the interface between liquid (melting zone) and solid (heat-impacted zone). This may be explained by the fact that Cr is less soluble in the  $\alpha$ -Ti or TiO phases than in the liquid phase [27], which causes the Cr atoms to be ejected into the liquid/solid interface during combustion. According to Ti-Cr phase diagrams [28], the segregation of 7 at.% Cr at the TC17 interface will result in a considerable reduction of  $\sim 70$  °C in the interfacial temperature  $T_m$ , whereas the segregation of Mo and Zr in TC11 results in an increase in the interfacial temperature.  $T_b$  can also be considered constant for the TC11 and TC17 alloys since it is determined by the peritectic reaction of the liquid phase and  $\alpha$ -Ti.  $T_s$  can also be considered constant, which is dependent on the heat transfer characteristics of alloys. As a result, the migration rate  $v$  in TC17 is larger than TC11 due to the drop in  $T_m$ . This implies that increasing the interfacial temperature by adding alloying elements is an advantageous strategy for lowering the combustion velocity of titanium alloys. Further investigation on the detailed combustion characteristics among typical titanium alloys will be conducted in our next work.

**Table 3.** Physical properties between TC17 and TC11 alloys [24–26].

	$\rho$ , g/m <sup>3</sup>	$c$ , J/(mol K)	$q$ , kJ/mol	$h$ , W/(m <sup>2</sup> °C)
TC17	4680	470	16~20	50
TC11	4480	544		

## 5. Conclusions

In this paper, the combustion behavior of the TC17 alloy, including ignition temperature, threshold oxygen pressure, and combustion kinetics, has been investigated by the promoted ignition–combustion (PIC) tests. The microstructure after extinguishing combustion has been further analyzed, and the impact of alloying elements on the combustion behavior has been further discussed. The following conclusions are drawn from this work:

- The combustion of the TC17 alloy consists of the ignition, splash, and flame propagation stages. The threshold oxygen pressure for the combustion of the TC17 alloy is comparable to that of TC11; however, the combustion velocity of the TC17 alloy is obviously faster. The combustion velocity and oxygen pressure follow a power law relationship;
- The oxide zone, melting zone, and heat-affected zone are observed in the TC17 alloy after extinguishing the combustion process. The segregation of Cr, Mo, and Al is

observed in the interdendritic phase in the melting zone and the interface between the melting zone and the heat-affected zone;

- The enhanced combustion velocity of the TC17 alloy may be caused by the segregation of Cr at the liquid/solid interface, which lowers the interfacial temperature and speeds up the migration of the liquid/solid interface.

**Author Contributions:** Conceptualization, C.Z.; methodology, P.X. and Z.L.; validation, C.Z., C.W. and G.H.; investigation, J.L. and B.W.; resources, J.H.; data curation, C.Z.; writing—original draft preparation, C.Z. and Z.L.; writing—review and editing, C.Z.; visualization, C.D. and Y.J.; supervision, C.Z.; project administration, J.H.; funding acquisition, C.Z. All authors have read and agreed to the published version of the manuscript.

**Funding:** This research was funded by Technology Fund of the Ministry of science and technology (grant number 2020-JCJQ-JJ-248), Fundamental Research Funds for the Central Universities (grant number FRF-GF-20-21B, FRF-TP-22-129A1), National Natural Science Foundation of China (grant number 52101072), National Science and Technology Projects of China (grant number J2019-VIII-0003-0164).

**Data Availability Statement:** Data presented in this article are available at request from the corresponding author.

**Conflicts of Interest:** The authors declare no conflict of interest.

## References

- Peters, M.; Kumpfert, J.; Ward, C.H.; Leyens, C. Titanium Alloys for Aerospace Applications. *Adv. Eng. Mater.* **2003**, *5*, 419–427. [[CrossRef](#)]
- Luo, Q.S.; Li, S.F.; Pei, H.P. Progress in Titanium Fire Resistant Technology for Aero-Engine. *J. Aerosp. Power* **2012**, *27*, 2763–2768.
- Shao, L.; Xie, G.; Zhang, C.; Liu, X.; Lu, W.; He, G.; Huang, J. Combustion of Metals in Oxygen-Enriched Atmospheres. *Metals* **2020**, *10*, 128. [[CrossRef](#)]
- Clark, A.F.; Moulder, J.C.; Runyan, C.C. Combustion of Bulk Titanium in Oxygen. *Symp. Combust.* **1975**, *15*, 489–499. [[CrossRef](#)]
- Littman, F.E.; Church, F.M.; Kinderman, E.M. A Study of Metal Ignitions I. The Spontaneous Ignition of Titanium. *J. Less Common Met.* **1961**, *3*, 367–378. [[CrossRef](#)]
- Yu, J.; Zhang, X.; Zhang, Q.; Wang, L.; Ji, K.; Peng, L.; Gao, W. Combustion Behaviors and Flame Microstructures of Micro- and Nano-Titanium Dust Explosions. *Fuel* **2016**, *181*, 785–792. [[CrossRef](#)]
- Dreizin, E.L. Phase Changes in Metal Combustion. *Prog. Energy Combust. Sci.* **2000**, *26*, 57–78. [[CrossRef](#)]
- Gaohui, Z.; Zhang, P.Z.; Guoqing, H.; Xu, P.; Shunqi, Z. Study on the Burn-Resistant Properties of Titanium Alloy Ti<sub>6</sub>Al<sub>4</sub>V Surface by Diffusing Copper. *Rare Met. Mater. Eng.* **2011**, *40*, 286–289.
- Molodetsky, I.E.; Vicenzi, E.P.; Dreizin, E.L.; Law, C.K. Phases of Titanium Combustion in Air. *Combust. Flame* **1998**, *112*, 522–532. [[CrossRef](#)]
- Shafirovich, E.; Teoh, S.K.; Varma, A. Combustion of Levitated Titanium Particles in Air. *Combust. Flame* **2008**, *152*, 262–271. [[CrossRef](#)]
- Schutz, R.W. Environmental Behavior of Beta Titanium Alloys. *J. Miner. Met. Mater. Soc.* **1994**, *46*, 24–29. [[CrossRef](#)]
- Bolobov, V.I.; Makarov, K.M.; Shteinberg, A.S.; Drozhzhin, P.F. Compact-Specimen Burning with Fresh Metal Surface Production. *Combust. Explos. Shock Waves* **1992**, *28*, 457–459. [[CrossRef](#)]
- Bolobov, V.I. Mechanism of Self-Ignition of Titanium Alloys in Oxygen. *Combust. Explos. Shock Waves* **2002**, *38*, 639–645. [[CrossRef](#)]
- Shao, L.; Xie, G.; Liu, X.; Wu, Y.; Yu, J.; Hao, Z.; Lu, W.; Liu, X. Combustion Behaviour and Mechanism of TC<sub>4</sub> and TC<sub>11</sub> Alloys. *Corros. Sci.* **2020**, *168*, 108564. [[CrossRef](#)]
- Shao, L.; Li, Z.; Yu, J.; Yang, G.; Zhang, C.; Zou, Y.; Huang, J. Combustion Behavior and Mechanisms of Ti<sub>2</sub>AlNb Compared to an  $\alpha + \beta$  Ti Alloy. *Corros. Sci.* **2021**, *192*, 109868. [[CrossRef](#)]
- Shao, L.; Wang, Y.; Xie, G.; Li, H.; Xiong, J.; Yu, J.; He, G.; Huang, J. Combustion Mechanism of Alloying Elements Cr in Ti-Cr-V Alloys. *Materials* **2019**, *12*, 3206. [[CrossRef](#)]
- Huang, L.J.; Wang, B.; Gao, Y. Investigation of TC<sub>4</sub> and TC<sub>11</sub> Titanium Alloys' Combustion Resistance Properties. *J. Mater. Eng.* **2004**, 33–35.
- Shao, L.; Xie, G.; Liu, X.; Wu, Y.; Tan, Q.; Xie, L.; Xin, S.; Hao, F.; Yu, J.; Xue, W.; et al. Combustion Behavior and Mechanism of Ti-25V-15Cr Compared to Ti-6Al-4V Alloy. *Corros. Sci.* **2022**, *194*, 109957. [[CrossRef](#)]
- Chen, Y.; Yang, W.; Bo, A.; Zhan, H.; Zhang, F.; Zhao, Y.; Zhao, Q.; Wan, M.; Gu, Y. Underlying Burning Resistant Mechanisms for Titanium Alloy. *Mater. Des.* **2018**, *156*, 588–595. [[CrossRef](#)]
- Chen, Y.; Huo, Y.; Song, X.; Bi, Z.; Gao, Y.; Zhao, Y. Burn-Resistant Behavior and Mechanism of Ti<sub>14</sub> Alloy. *Int. J. Miner. Metall. Mater.* **2016**, *23*, 215–221. [[CrossRef](#)]
- Ding, M.C.; Zhang, Y.L.; Lu, H.T. Fatigue Life Prediction of TC17 Titanium Alloy Based on Micro Scratch. *Int. J. Fatigue* **2020**, *139*, 105793. [[CrossRef](#)]

22. Liang, S.; Li, J.; Zhang, Q.; Chen, J. Microstructural Evolution in the TC17 Titanium Alloy Processed During Laser Stereo Forming. *J. Mater. Eng. Perform.* **2021**, *30*, 2967–2976. [[CrossRef](#)]
23. Sato, J.; Hirano, T. Fire Spread Limits along Metal Pieces in Oxygen. In *Flammability and Sensitivity of Materials in Oxygen-Enriched Atmospheres: Third Volume, ASTM STP, 986*; ASTM: Philadelphia, PA, USA, 1988; pp. 158–171. [[CrossRef](#)]
24. Zhao, P.; Fu, L.; Zhong, D. Numerical Simulation of Transient Temperature and Axial Deformation during Linear Friction Welding between TC11 and TC17 Titanium Alloys. *Comput. Mater. Sci.* **2014**, *92*, 325–333. [[CrossRef](#)]
25. Xie, L.; Liu, C.; Song, Y.; Guo, H.; Wang, Z.; Hua, L.; Wang, L.; Zhang, L.C. Evaluation of Microstructure Variation of TC<sub>11</sub> Alloy after Electroshocking Treatment. *J. Mater. Res. Technol.* **2020**, *9*, 2455–2466. [[CrossRef](#)]
26. Yang, Y.; Zhang, H.; Qiao, H. Microstructure Characteristics and Formation Mechanism of TC17 Titanium Alloy Induced by Laser Shock Processing. *J. Alloys Compd.* **2017**, *722*, 509–516. [[CrossRef](#)]
27. Chepulskii, R.V.; Curtarolo, S. Calculation of Solubility in Titanium Alloys from First Principles. *Acta Mater.* **2009**, *57*, 5314–5323. [[CrossRef](#)]
28. Murray, J.L. The Cr–Ti (Chromium-Titanium) System. *Bull. Alloy Phase Diagr.* **1981**, *2*, 174–181. [[CrossRef](#)]

**Disclaimer/Publisher’s Note:** The statements, opinions and data contained in all publications are solely those of the individual author(s) and contributor(s) and not of MDPI and/or the editor(s). MDPI and/or the editor(s) disclaim responsibility for any injury to people or property resulting from any ideas, methods, instructions or products referred to in the content.